

A BCS Gapped Superfluid on the Lattice

David N. WALTERS*)

*Theoretical Physics Group, Department of Physics and Astronomy, **)*

University of Manchester, Manchester M13 9PL, UK

and

Department of Physics, University of Wales Swansea,

Singleton Park, Swansea SA2 8PP, UK

We discuss results of numerical analyses of the 3+1 dimensional Nambu–Jona-Lasinio model at non-zero baryon density. By studying relevant order parameters, it is shown that the model goes through a transition between a vacuum with broken chiral symmetry, and a chirally restored phase at high baryon chemical potential μ with a diquark condensate roughly proportional to the area of the Fermi surface and a broken $U(1)$ baryon number symmetry. The condensation of diquark pairs from the fermionic spectrum is shown to lead to an energy gap Δ about the Fermi energy E_F , which is found to be $\approx 15\%$ of the vacuum fermion mass and roughly independent of μ in the chirally restored phase. The ground-state is believed, therefore, to be that of a BCS superfluid. We also discuss the effect of simulating on a finite volume, and any caveats this places on the conclusions made above.

§1. Introduction

The physics of compact stars is a field that has attracted much interest in recent years. At zero temperature, deconfined quark matter within the core of these objects is believed to be unstable with respect to a ground-state in which quark (and hole) pairs in the region of the Fermi surface condense out of the spectrum in a manner analogous to that in the BCS theory of superconductivity; because diquark pairs cannot be colour singlet, this phenomenon is known as colour superconductivity (CSC).¹⁾ The simplest CSC ground-state, known as 2SC, is one in which condensation occurs between the approximately degenerate u and d quarks, leaving an energy gap 2Δ about the Fermi surface in their spectra. The fact that the force between quarks in QCD is strongly attractive means that estimates for the magnitude of Δ can be as large as 50–100 MeV, i.e. large enough to remain present at typical compact star temperatures of $\mathcal{O}(1\text{MeV})$.²⁾

The confirmation of this picture by a first principles lattice QCD calculation, however, remains elusive due to the difficulties of performing Monte-Carlo simulations with baryon chemical potential $\mu \neq 0$. Whilst the “sign problem” remains, the only way of probing the cold, dense region of the QCD phase diagram non-perturbatively is by using model field theories, such as 2 colour QCD or the Nambu–Jona-Lasinio (NJL) model.

In both of these models, the functional weight remains both real and positive, even with $\mu \neq 0$,^{3),4)} such that they are simulable using standard lattice techniques.

*) This work was completed with the support of PPARC and in collaboration with Simon Hands. Thanks also go to Tom Kingaby for enlightening discussions.

**) Current address.

Lattice simulations of the NJL model show that chiral symmetry restoration occurs at some critical chemical potential $\mu_c \sim \Sigma_0$, where Σ_0 is the constituent quark mass, in qualitative agreement with analytic approaches such as the large- N_c (or Hartree) approximation.⁵⁾ Furthermore, whilst this model has no gauge degrees of freedom and cannot describe confined matter, the fundamental quarks that play the rôle of the baryons do obey the correct statistics, such that the effect of increasing μ beyond μ_c is to build up a Fermi surface. This should be contrasted with 2 colour QCD, in which the qq baryons are bosonic and the onset of matter occurs at $\mu_c \sim m_\pi/2$. Together, these features make the lattice NJL model an ideal tool with which to study Fermi surface phenomena, such as CSC, at phenomenologically relevant densities.

§2. The model

The model studied herein is the 3+1 dimensional lattice NJL model, which in continuum notation has the Euclidean Lagrangian

$$\begin{aligned} \mathcal{L} = & \bar{\psi}(\not{\partial} + m + \mu\gamma_0)\psi \\ & - \frac{g^2}{2} \left[(\bar{\psi}\psi)^2 - (\bar{\psi}\gamma_5 \otimes \vec{\tau} \otimes \gamma_5\psi)^2 \right] \\ & + \frac{1}{2} \left[(\bar{\psi}, \psi^{tr}) \begin{pmatrix} j & \\ & j \end{pmatrix} C\gamma_5 \otimes \tau_2 \otimes C\gamma_5 \begin{pmatrix} \bar{\psi}^{tr} \\ \psi \end{pmatrix} \right], \end{aligned} \quad (2.1)$$

where m is the bare- or current-quark mass, and the source j has been added to allow the measurement of a baryon number violating diquark condensate in a finite volume system.

When formulated on a discrete lattice of sites x with separation a between nearest neighbours, the model is described in terms of the staggered fermion fields $\chi, \bar{\chi}, \zeta$ and $\bar{\zeta}$ by the action

$$S = a^4 \sum_x \left[(\bar{\chi}, \chi^{tr}) \mathcal{A} \begin{pmatrix} \bar{\chi}^{tr} \\ \chi \end{pmatrix} + (\bar{\zeta}, \zeta^{tr}) \mathcal{A}^* \begin{pmatrix} \bar{\zeta}^{tr} \\ \zeta \end{pmatrix} \right] + \frac{2a^4}{g^2} \sum_{\tilde{x}} (\sigma^2 + \vec{\pi} \cdot \vec{\pi}), \quad (2.2)$$

where \mathcal{A} is the Nambu-Gor'kov matrix

$$\mathcal{A} = \frac{1}{2} \begin{pmatrix} j\tau_2^{pq} & M \\ -M^{tr} & j\tau_2^{pq} \end{pmatrix}. \quad (2.3)$$

In turn, M is the fermion kinetic matrix

$$\begin{aligned} M_{xy}^{pq} = & \frac{1}{2a} \delta^{pq} \left[\left(e^{a\mu} \delta_{yx+\hat{0}} - e^{-a\mu} \delta_{yx-\hat{0}} \right) + \sum_{\nu=1}^3 \eta_\nu(x) (\delta_{yx+\hat{\nu}} - \delta_{yx-\hat{\nu}}) + 2am\delta_{xy} \right] \\ & + \frac{1}{16} \delta_{xy} \sum_{\langle \tilde{x}, x \rangle} (\sigma(\tilde{x})\delta^{pq} + i\epsilon(x)\vec{\pi}(\tilde{x}) \cdot \vec{\tau}^{pq}), \end{aligned} \quad (2.4)$$

where $\vec{\tau}^{pq}$ is a vector of the Pauli matrices which act on the $N_f = 2$ isospin degrees of freedom. The lattice model also exhibits an additional $N_c = 8$ “colour” degrees of

freedom, due to staggered fermion doubling and the choice of (2.2). The auxiliary scalar and pseudoscalar fields σ and $\vec{\pi}$ are defined on sites \tilde{x} of a dual lattice, $\langle \tilde{x}, x \rangle$ represent the sum over the 16 dual sites neighbouring x , and the symbols $\eta_\nu(x)$ and $\epsilon(x)$ are the phases $(-1)^{x_0+\dots+x_{\nu-1}}$ and $(-1)^{x_0+x_1+x_2+x_3}$ respectively.

In the limit that m and $j \rightarrow 0$, (2.2) has the same global symmetries as QCD with two massless flavours, i.e. the $SU(2)_L \otimes SU(2)_R$ chiral symmetry of left- and right-handed quarks

$$\begin{aligned} \chi &\rightarrow (P_L U + P_R V) \chi; & \bar{\chi} &\rightarrow \bar{\chi} (P_L V^\dagger + P_R U^\dagger); \\ \zeta &\rightarrow (P_L V + P_R U) \zeta; & \bar{\zeta} &\rightarrow \bar{\zeta} (P_L U^\dagger + P_R V^\dagger); \\ (\sigma + i\vec{\pi} \cdot \vec{\tau}) &\rightarrow V(\sigma + i\vec{\pi} \cdot \vec{\tau}) U^\dagger, \end{aligned} \quad (2.5)$$

where $P_{L,R} \equiv \frac{1}{2}(1 \pm \epsilon(x))$ and U and V are elements of $SU(2)$, and the $U(1)_B$ symmetry of baryon number

$$\chi \rightarrow e^{i\alpha} \chi, \quad \bar{\chi} \rightarrow e^{-i\alpha} \bar{\chi}. \quad (2.6)$$

As in QCD, at $\mu = 0$ chiral condensation leads the spontaneous generation of a constituent quark mass $\Sigma_0 \gg m$ which breaks $SU(2)_L \otimes SU(2)_R$ down to the $SU(2)_I$ of isospin. These reassuring features suggest that by studying the model's global symmetries and their breaking, we can learn about the analogous symmetry breaking patterns in QCD.

In 3+1 dimensions the NJL model is only an effective theory, such that the lattice parameters must be chosen to match low energy phenomenology. By applying the large- N_c (Hartree) approximation analytically to staggered quarks, we determine a suitable set, leading to physically reasonable results, to be

$$\begin{aligned} am &= 0.006 & \Sigma_0 &= 400 \text{ MeV} \\ a^2 g^{-2} &= 0.495 & f_\pi &= 93 \text{ MeV} \\ a^{-1} &= 720 \text{ MeV} & m_\pi &= 138 \text{ MeV}. \end{aligned} \quad (2.7)$$

§3. Order parameters

In previous work,⁶⁾ we have performed simulations of the model outlined in §2 in an attempt to identify diquark condensation in the dense phase. In particular, we measure the diquark condensate

$$\langle qq \rangle \equiv \frac{1}{2V} \frac{\partial \ln \mathcal{Z}}{\partial j} = \frac{1}{8V} \left\langle \text{Tr} \begin{pmatrix} \tau_2 & \\ & \tau_2 \end{pmatrix} \mathcal{A}^{-1} \right\rangle, \quad (3.1)$$

where \mathcal{Z} is the partition function, and compare it to the chiral condensate

$$\langle \bar{q}q \rangle \equiv \frac{1}{V} \frac{\partial \ln \mathcal{Z}}{\partial m} = \frac{1}{4V} \left\langle \text{Tr} \begin{pmatrix} & \mathbb{1}_2 \\ -\mathbb{1}_2 & \end{pmatrix} \mathcal{A}^{-1} \right\rangle. \quad (3.2)$$

We perform simulations for a range of μ on $V = L_t \times L_s^3$ lattices with $L_t = L_s = 12, 16$ and 20 using a standard hybrid Monte-Carlo (HMC) algorithm, in which the

source strength is set to zero during the update of the auxiliary background fields, but allowed to vary over a range of $j = j^* \neq 0$ during the quenched measurement of the quantities above. An interesting empirical observation is that results in the chiral sector are found to scale linearly with inverse volume, whilst diquark observables scale with inverse temporal extent, which in Euclidean space corresponds to the temperature. Accordingly, $\langle \bar{q}q \rangle$ is extrapolated to $V^{-1} \rightarrow 0$, whilst $\langle qq \rangle$ is extrapolated first to $L_t^{-1} \rightarrow 0$ and then $j \in [0.3, 1.0] \rightarrow 0$.*) The results are plotted in Fig. 1. As expected, at $\mu = 0$ chiral symmetry is broken leading to a non-zero chiral

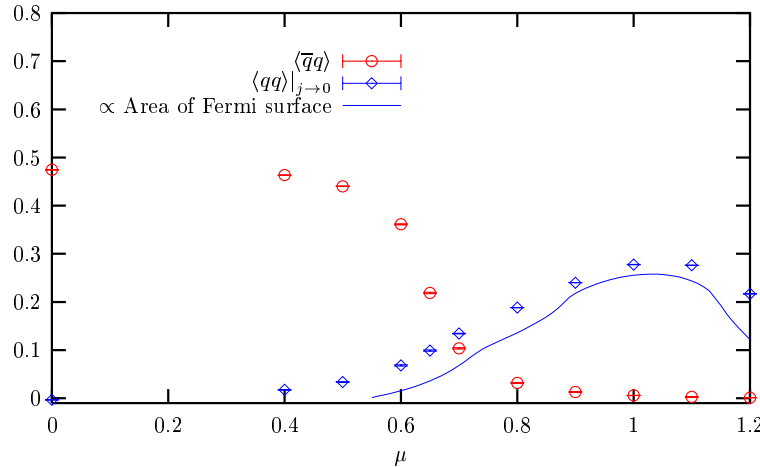


Fig. 1. Order parameters as functions of μ . The solid line represents the area of the Fermi surface calculated in the large- N_c limit.

condensate whilst $\langle q\bar{q} \rangle \simeq 0$. As chemical potential is increased, the system goes through a crossover into a phase with approximate chiral symmetry restoration and a non-zero diquark condensate. In particular, $\langle q\bar{q} \rangle$ is found to increase roughly as the area of the lattice Fermi surface, plotted in arbitrary units for free fermions in the large- N_c limit as the solid curve. This supports the naïve picture of the condensate being a measure of the density of pair states about the Fermi surface, contributing to diquark condensation.

§4. The superfluid gap

In the previous section, we presented evidence for superfluidity in the form a non-zero diquark condensate in the high- μ phase. This evidence must be treated as indirect, however, since this quantity is not measurable in an experiment. Furthermore, even if the sign problem were overcome, one could not measure $\langle q\bar{q} \rangle$ in lattice QCD, since in this theory the colour superconducting phase is characterised by the breaking of a gauge symmetry; Elitzur's theorem states that one cannot define a local order parameter to distinguish the existence of such a phase in a gauge invari-

*) Although all diquark observables are measured for $0.1 \leq j \leq 1.0$, the behaviour of data with $j < 0.3$ appears to disagree markedly with that of those at higher j , and these are ignored for the purposes of these fits. We attribute this to finite volume errors, which we discuss briefly in §5.

ant way.⁷⁾ Instead, we turn to more direct evidence in the form of the global order parameter for the BCS phase, the energy gap Δ .

We do this by studying the fermionic dispersion relation $E(k)$, extracted from the Gor'kov time-slice propagator

$$\mathcal{G}(\vec{k}, t) \equiv \sum_{\vec{x}} \mathcal{A}^{-1}(\vec{0}, 0; \vec{x}, t) e^{-i\vec{k} \cdot \vec{x}}, \quad (4.1)$$

on $L_t \times L_x \times L_{y,z}^2$ lattices with $L_t = 16, 20$ and 24 , $L_x = 96$ and $L_{y,z} = 12$. The momenta sampled are $\vec{k} = (2\pi n/L_x, 0, 0)$ for $n = 0, 1, 2, \dots$, implying that for our choice of lattices there are 25 independent momentum modes between $k = 0$ and $\pi/2$ in the k_x direction. We measure \mathcal{G} at $\mu = 0.8$ for a range of j , using standard lattice methods for meson correlators, in the same partially quenched approximation employed in the measurement of the order parameter. It is found empirically that whilst in general \mathcal{G} has 16 complex components in Nambu-Gor'kov space, only two parts of these are independent and non-zero. These are

$$N(k, t) \equiv \text{Re}(\mathcal{G}_{13}(k, t)) \quad \& \quad A(k, t) \equiv \text{Im}(\mathcal{G}_{21}(k, t)), \quad (4.2)$$

which in the limit that $j \rightarrow 0$ correspond to the propagators for particles

$$N(k, t) \sim \langle q(x) \bar{q}(y) \rangle_{11} \quad (4.3)$$

and for superpositions of particles and holes

$$A(k, t) \sim \langle q(x) q(y) \rangle_{21}. \quad (4.4)$$

We label these the ‘‘normal’’ and ‘‘anomalous’’ propagators respectively. Fitting these to

$$N(k, t) = A e^{-Et} + B e^{-E(L_t - t)} \quad (4.5a)$$

$$A(k, t) = C(e^{-Et} - e^{E(L_t - t)}) \quad (4.5b)$$

we extract the amplitudes $A(k, j)$, $B(k, j)$ and $C(k, j)$ and the excitation energy $E(k, j)$, and as with $\langle qq \rangle$ extrapolate to $L_t^{-1} \rightarrow 0$ and then $j \in [0.3, 1.0] \rightarrow 0$.

Fig. 2 shows the amplitudes A , B and C as functions of j in the limit $T, j \rightarrow 0$. At low k , $A \gg B$ corresponding to a predominantly forward moving signal, which implies that the normal propagator deep within the Fermi sea is dominated by hole-like excitations. At large k the reverse is true, implying that excitations above the Fermi surface are

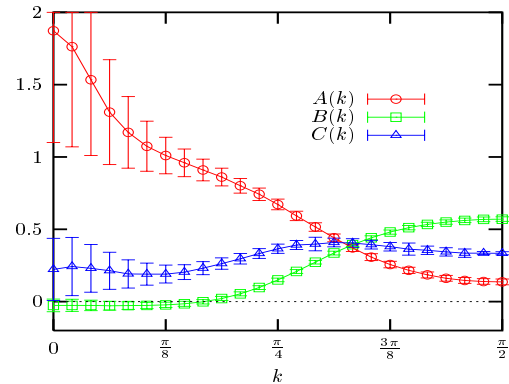


Fig. 2. Propagator amplitudes at $\mu = 0.8$.

dominated by particles. The point at which $A(k)$ and $B(k)$ coincide, therefore, can be identified with the momentum at the Fermi surface, k_F .⁴⁾ Of particular interest is the fact that the coefficient for the anomalous propagator $C(k)$ is non-zero in a broad peak about k_F , even in the $j \rightarrow 0$ limit, which implies that there are particle-hole mixed states with indefinite baryon number, an indirect signal for superfluidity via a BCS mechanism.

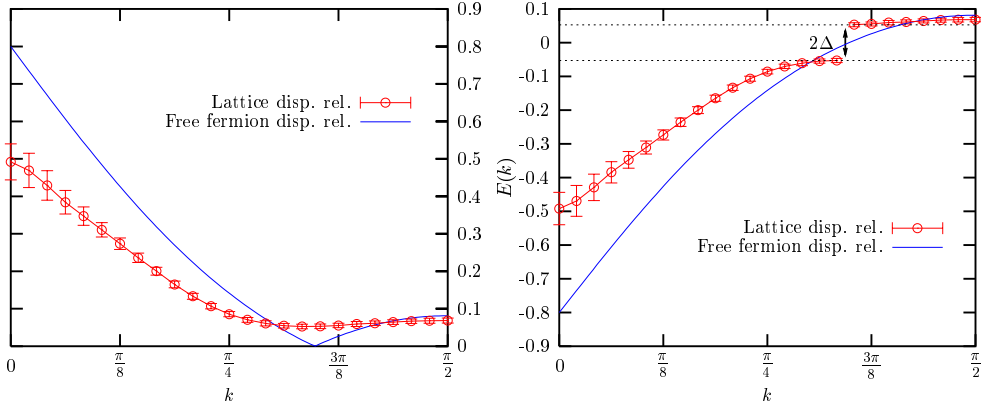


Fig. 3. Lattice dispersion relation and typical free fermion dispersion relation at $\mu = 0.8$.

The left-hand panel of Fig. 3 shows the fermion dispersion relation at $\mu = 0.8$, i.e. the energy of the fermionic excitations as a function of their momenta, compared to that of non-interacting lattice fermions. The free fermion dispersion relation clearly has two branches, representing hole excitations for $k < k_F$ and particle excitations for $k > k_F$. In between one observes that $E(\sin^{-1}(\sinh(\mu a))) = 0$. In contrast to this, in the dispersion relation extracted from the lattice data one can see no discontinuity between the two branches, another sign of particle-hole mixing. More importantly, at no point does $E(k)$ pass through $E = 0$ and there is a distinct gap between this point and the minimum.

This can be seen in a more familiar light if one plots the hole branch as negative, which is done in the right-hand panel of Fig. 3. This makes the free fermion dispersion relation a smooth continuous curve, which is similar to those observed in lattice theories with no BCS gap,^{4),8)} whilst for our smooth dispersion relation this introduces a discontinuity at $k \approx k_F$ signalling an energy gap 2Δ . This is the first direct observation of a BCS gap in a lattice simulation.

In order to learn something of the chemical potential dependence of the gap we perform a naïve extrapolation of data extracted from $L_t = 16$ and 20 lattices to zero temperature and assign a conservative estimate of the error; the $L_t = 24$ data required for a full statistical treatment such as that applied at $\mu = 0.8$ are too expensive to reproduce for a range of μ in the chirally restored phase. Data are then extrapolated to $j \rightarrow 0$ as before so that we can plot the dispersion relations and gain an estimate for the gap. These are plotted in the left-hand panel of Fig. 4. It is worth noting that whilst a linear extrapolation through two points is of little statistical value, the results produced at $\mu = 0.8$ with and without using the $L_t = 24$

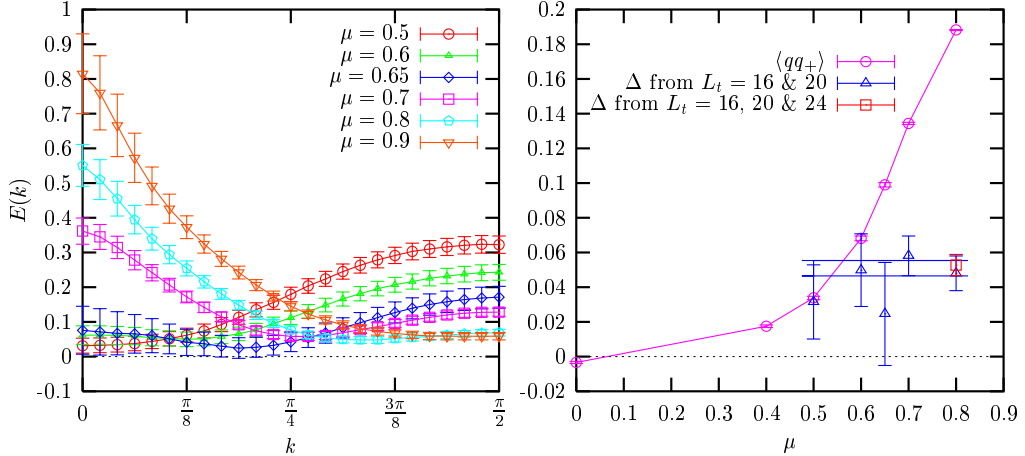


Fig. 4. Lattice dispersion relations at various values of μ and a comparison between their minima and the diquark condensate.

data are found to be consistent for all k .

The estimates for $\Delta(\mu)$ are plotted in the right-hand panel of Fig. 4, which shows that Δ appears roughly constant for $\mu > \mu_c$, whilst $\langle qq \rangle$ rises with the area of the Fermi surface. This is consistent with the simple-minded assumption that the order parameter counts the density of states from within a shell of thickness $\mathcal{O}(\Delta)$ about the Fermi surface that contribute to diquark condensation, such that in the continuum

$$\langle qq \rangle \propto \Delta \mu^2. \quad (4.6)$$

Finally, in order to express our best measurement of the gap, $\Delta a(\mu a = 0.8) = 0.053(6)$, in a form independent of the lattice spacing a , we extract the vacuum fermion mass Σ_0 from simulations with $L_t = 16, 20$ and 24 and find

$$\frac{\Delta}{\Sigma_0} = 0.15(2). \quad (4.7)$$

Assuming that $\Sigma_0 \sim 400$ MeV, this implies that in physical units, the size of the gap is $\Delta \sim 60$ MeV, which is consistent with the predictions of Ref. 2).

§5. Finite volume effects

An important point that we have failed, thus far, to highlight is that the conclusions of the previous sections rely on the disregarding of data with $j < 0.3$, for which the order parameter and other diquark observables deviate sharply from the fitted form. We attribute this to finite volume errors, which are particularly large in this system,⁹⁾ a fact we believe to be due to the difficulty of representing a small shell of states close to the Fermi surface on a discrete momentum-mode lattice. To address this issue, parallel simulations are currently being attempted on very large lattices, with the aim of showing that on such systems the deficiency at low- j is reduced. Thusfar, these simulations have proven hard, with very small time-steps

and trajectories required for acceptance rates of over 50%. This might be interpreted as a sign of encouragement, however, as the failure of the algorithm may be a signal that the partially quenched approximation is insufficient for such large volumes. If the volume is large enough that the proposed finite size effects are overcome, there may be enough momentum modes within the shell about the Fermi surface for di-quark condensation to occur even with $j \equiv 0$, as partial quenching enforces during the field updates. The algorithm would then be attempting to represent a system with an exact Goldstone mode and encounter the standard finite size effects related to divergent Goldstone fluctuations. A full simulation, with $j \neq 0$ during all steps of the algorithm, may yet be required to resolve this issue.

§6. Summary

To summarise, our evidence for s-wave superfluidity via a BCS instability is of some importance, since this is the first time that the presence of such a phase has been demonstrated in a relativistic quantum field theory using a systematic calculational technique. Although the $3 + 1d$ NJL model is only a simplistic effective field theory, this work can be interpreted phenomenologically as non-perturbative evidence for BCS colour superconductivity in QCD with two degenerate flavours, since these two theories have the same global symmetry structure. This is of particular importance whilst the persistence of the sign problem prevents the numerical solution of full $SU(3)$ QCD. Also, the fact that our results agree with the predictions of self-consistent treatments of this simple model adds credence to solutions of similar models with more complicated flavour structures and interactions.

In future work it would be interesting to further this analysis to study the stability of the superfluid phase by performing simulations either at non-zero temperature with the aim of measuring the critical temperature of the superfluid phase, or with the Fermi surfaces for “up” and “down” quarks separated via the introduction of a small non-zero isospin chemical potential. The latter option may be difficult, however, since initial studies indicate that with this introduction, $\det M$ becomes complex.

The most pressing issue, however, is to resolve the finite volume effects discussed above, since it is only once this issue has been addressed that the conclusions of §3 & §4 may be trusted completely.

References

- 1) For recent reviews see: K. Rajagopal and F. Wilczek, in: M. Shifman (ed.) *Handbook of QCD*, ch. 35, World Scientific, 2001, [arXiv:hep-ph/0011333](https://arxiv.org/abs/hep-ph/0011333); M.G. Alford, Ann. Rev. Nucl. Part. Sci. **51** (2001) 131.
- 2) J. Berges and K. Rajagopal, Nucl. Phys. **B538** (1999) 215.
- 3) S.J. Hands, I. Montvay, L. Scorzato and J. Skullerud, Eur. Phys. J. **C22** (2001) 451.
- 4) S.J. Hands, B. Lucini and S. Morrison, Phys. Rev. **D65** (2002) 036004.
- 5) S.P. Klevansky, Rev. Mod. Phys. **64** (1992) 649.
- 6) S.J. Hands and D.N. Walters, Phys. Lett. **B548** (2002) 196.
- 7) S. Elitzur, Phys. Rev. **D12** (1975) 3978.
- 8) S.J. Hands, J.B. Kogut, C.G. Strouthos and T.N. Tran, Phys. Rev. **D68** (2003) 016005.
- 9) P. Amore, M.C. Birse, J.A. McGovern and N.R. Walet, Phys. Rev. **D65** (2002) 074005.